



# CHORUS

This is the accepted manuscript made available via CHORUS. The article has been published as:

## Partial demixing of RNA-protein complexes leads to intradroplet patterning in phase-separated biological condensates

Kelsey Gasior, Jia Zhao, Grace McLaughlin, M. Gregory Forest, Amy S. Gladfelter, and Jay Newby

Phys. Rev. E **99**, 012411 — Published 10 January 2019

DOI: [10.1103/PhysRevE.99.012411](https://doi.org/10.1103/PhysRevE.99.012411)

# Partial demixing of RNA-protein complexes leads to intra-droplet patterning in phase-separated biological condensates

Kelsey Gasior<sup>1,+</sup>, Jia Zhao<sup>2,+</sup>, Grace McLaughlin<sup>1</sup>, Greg Forest<sup>3,4,5</sup>, Amy S. Gladfelter<sup>1,\*</sup>, and Jay Newby<sup>6,\*</sup>

<sup>1</sup>University of North Carolina at Chapel Hill Department of Biology, Coker Hall CB #3280, 120 South Rd, Chapel Hill, NC 27514, USA

<sup>2</sup>Utah State University, Animal Science 108, 3900 Old Main Hill, Logan, UT 84322, USA

<sup>3</sup>University of North Carolina at Chapel Hill Department of Mathematics, 329 Phillips Hall CB #3250, Chapel Hill, NC 27514, USA

<sup>4</sup>University of North Carolina at Chapel Hill & North Carolina State University Joint Department of Biomedical Engineering, 333 S Columbia St, Chapel Hill, NC 27514, USA

<sup>5</sup>University of North Carolina at Chapel Hill Department of Applied Physical Sciences, 1112 Murray Hall, CB#3050, Chapel Hill, NC 27514, USA

<sup>6</sup>Department of Mathematical and Statistical Sciences, CAB 632, University of Alberta, Edmonton, Alberta, Canada T6G 2G1

+These authors contributed to the work equally.

\*Corresponding authors

## Email Addresses

kgasior@email.unc.edu

jia.zhao@usu.edu

gamclaug@live.unc.edu

forest@unc.edu

amyglad@unc.edu

jnewby@ualberta.ca

## Key Words:

Liquid-liquid phase separation

RNA-protein bodies

Patterning

Cellular Organization

## Abstract

An emerging mechanism for intracellular organization is liquid-liquid phase separation (LLPS). Found in both the nucleus and the cytoplasm, liquid-like droplets condense to create compartments that are thought to promote and inhibit specific biochemistry. In this work, a multiphase, Cahn-Hilliard diffuse interface model is used to examine RNA-protein interactions driving LLPS. We create a bivalent system that allows for two different species of protein-RNA complexes and model the competition that arises for a shared binding partner, free protein. With this system we demonstrate that the binding and unbinding of distinct RNA-protein complexes leads to diverse spatial pattern formation and dynamics within droplets. Both the initial formation and transient behavior of spatial patterning are subject to the exchange of free proteins between RNA-protein complexes. This study illustrates that spatiotemporal heterogeneity can emerge within phase-separated biological condensates with simple binding reactions and competition. Intra-droplet patterning may influence droplet composition and, subsequently, cellular organization on a larger scale.

## Introduction

Liquid-liquid phase separation (LLPS) has emerged as a common mechanism for intracellular organization [1, 2]. Liquid-like condensates create cellular compartments akin to but quite different from those bound by lipid bilayer membranes [3]. Droplet formation is thought to be driven by LLPS and therefore assembly and disassembly can be far more dynamically controlled than membrane-bound compartments [4, 5]. Found in both the nucleus (e.g., the nucleolus, Cajal bodies, and PML bodies) and the cytoplasm (e.g., stress granules, P-bodies, and P-granules), these liquid droplet compartments sequester condensates of specific molecular ingredients and their complexes [6-8]. The droplets create localized environments that are hypothesized to functionally serve to promote or inhibit specific biochemistry, and to sequester RNAs and proteins within the compartment [9, 10]. In many cases, intrinsically disordered proteins with polyQ tracts, prion-like domains or low-complexity sequences promote phase separation and frequently these disordered domains are coupled to multiple RNA binding domains [7, 11, 12]. Additionally, multiple proteins are capable of attaching to a single RNA in the RNA-protein complexes [2, 13, 14]. This multivalency of RNA-protein interactions provides a physical basis, analogous to polymeric phase separation, for RNA-protein complexes and free species to undergo LLPS as explored in the above references.

The molecular interactions that promote LLPS have been explored through mathematical modeling using simple systems of soluble and phase-separating constituents [15-18]. While employing both sharp and diffuse interface techniques, many of these studies primarily focused on macroscale changes that result from transient molecular interactions, such as droplet formation and spatial patterning [15-19]. A key challenge is to resolve how chemical reactions arrest Ostwald ripening by pushing the system away from equilibrium via catalytic cores, externally controlled reactions, and optimized reversible reaction rates [17, 19, 20]. Other work has considered multiple reacting volume fractions to address the question of how phase separation works under generic biological conditions, where many molecular species coexist in a crowded mixture. These studies consider random interaction potentials among a large number of species [7]. While these models have examined the role of specific molecular interactions on multi-step complex formation and intra-droplet pattern formation [7], the influence of different reversible molecular interactions on intra-droplet patterning has not been carefully explored by

modeling of LLPS in biological contexts. This is a critical gap because specificity in molecular interactions is likely central to regulating assembly and disassembly of diverse and distinct condensates that coexist in the same crowded cytoplasm [2] or nucleus [21].

The multivalent nature of RNA-protein interactions raises the possibility of multiple distinct protein-RNA complexes inhabiting the same phase-separated RNA droplet. While partial demixing has been proposed as a theoretical possibility [7], the implications for the dynamics and patterning of LLPS is not yet well explored through mathematical modeling. Specifically, a framework is needed, and is presented here, to examine the interplay between the kinetic timescales for reversible formation of multiple molecular complexes, the dynamics of phase separation, and the diffusive motion of all molecular species. This modeling framework provides predictions of dynamic spatial patterning of molecular species and complexes *within* phase-separated droplets, as well as the timescales for coarsening and ripening.

Herein, we present a phase field model that examines how the formation of protein and RNA complexes that compete for common components influences spatial and temporal dynamics of phase separation. We use a Cahn-Hilliard diffuse interface model [22] to describe both the droplet and the surrounding solution. As a foundation for tracking distinct protein-RNA complexes and their interactions and structure within single phase-separated droplets, we create a bivalent system that allows for two different species of protein-RNA complexes and model their respective volume fractions. While this model can be extended to additional complexes and multivalent interactions, we opt for simplicity at this point until such time that we have sufficiently resolved experimental data for the number and prevalence of higher-order complexes in phase-separated droplets. We assume each complex has the same interaction potential with the solution, favoring partial de-mixing in two-component droplets. The free RNA and protein precursors are assumed to mix freely within droplets and the surrounding solution, and therefore modeled as purely diffusive species (possibly with phase-dependent diffusivity).

Under these conditions, we model the competition that arises for a shared binding partner, free protein, when RNA is bivalent, and explore the dynamics and structure among four allowable species (free protein and RNA, RNA-protein and protein-RNA-protein complexes). With this reaction-diffusion system, and a chemical potential that favors phase separation, we demonstrate that the relative binding-unbinding kinetics of distinct RNA-protein complexes tunes the competition, leading to diverse spatial pattern formation and dynamics of patterns within individual droplets. Both the initial formation and transient behavior of spatial patterning are subject to the exchange of free proteins between RNA-protein complexes – behavior that is enhanced when protein and RNA mobility is phase dependent. The diverse patterning outcomes are captured with state diagrams of the initial, intermediate, and long-time dynamics and structure within phase-separated droplets, over a selected two-parameter space of binding-unbinding kinetics. This approach creates a general modeling framework upon which to add further complexity of molecular interactions relevant to multivalent systems involved in LLPS. The present bivalent RNA-protein model simulations study already illustrate and give insight into the diversity of spatiotemporal heterogeneity possible within phase-separated biological condensates, and provide feedback for future experiments.

### **Mathematical model of the kinetics of transient molecular interactions and spatial patterning of multiple (two) RNA-protein complexes**

We present a proof-of-principle model that examines the competition and behavior of two distinct protein-RNA complexes. As illustrated in Figure 1, a single protein (P) is capable of

binding with a single RNA (R), to form a simple protein-RNA complex ( $N_1$ ). If a different protein site on the RNA of the  $N_1$  complex binds with a second protein, the protein-RNA-protein complex ( $N_2$ ) is formed. Both the protein-RNA ( $N_1$ ) and protein-RNA-protein ( $N_2$ ) complexes are capable of driving droplet formation and coexist within a droplet,



The Cahn-Hilliard phase field model allows us to use an order parameter ( $\phi$ ) to describe the matrix ( $\phi = 0$ ), the droplet ( $\phi = 1$ ), and the interface ( $0 < \phi < 1$ ) [23]. We decompose the order parameter as a multi-component mixture with  $\phi = N_1 + N_2$  consisting of the sum of volume fractions (in our bivalent model with  $N_1$  and  $N_2$ ) of the different complexes capable of forming due to protein-RNA binding interactions. For simplicity, we assume that the volume fraction for each component includes the required solvent. The volume fractions of the free RNA (denoted as R) and protein (denoted as P) are assumed to mix freely within the matrix and droplets with no interaction potential. We therefore assume that these variables evolve with standard Fickian diffusive dynamics [24]. As shown in Equations (1)—(5), the model couples the Cahn-Hilliard phase field model with reversible protein and RNA interactions (under detailed balance conditions) to describe the binding-unbinding of protein and RNA to form complexes capable of phase separation.

We assume that, initially, there are no protein-RNA complexes ( $N_1(x, 0) = N_2(x, 0) = 0$ ). It is also assumed that the system begins with a set amount of protein and RNA available for complex formation, that the system begins in normal physiological conditions, and that the volumes of RNA and protein are equal. Using the molecular weights of an  $\sim 1600$  nucleotide RNA and  $\sim 78$  kDA protein, these equal volume fractions would result in having roughly 6.5x as much protein available in the system as RNA. Further, it is assumed that the total volume of protein and RNA are conserved, resulting in a system wherein  $N_1$  and  $N_2$  formation must compete for limited resources, such as would exist in an *in vitro* experiment. The parameter definitions are given in Table 1. This model also assumes that the binding of protein to RNA does not result in structural changes that would affect kinetic rates or diffusivities. We denote the volume fractions for protein-RNA complex, protein-RNA-protein complex, free protein and free RNA by  $N_1, N_2, P$  and  $R$  respectively. Then the governing equations are proposed as

$$\frac{\partial N_2}{\partial t} = \nabla \cdot \left( \lambda_{N_2} M(\phi) \nabla \left( \frac{\delta F}{\delta N_2} \right) \right) + c_3 N_1 P - c_4 N_2, \quad (1)$$

$$\frac{\partial N_1}{\partial t} = \nabla \cdot \left( \lambda_{N_1} M(\phi) \nabla \left( \frac{\delta F}{\delta N_1} \right) \right) + c_1 P R - c_2 N_1 - c_3 N_1 P + c_4 N_2, \quad (2)$$

$$\frac{\partial P}{\partial t} = \nabla \cdot (\lambda_P M(\phi) \nabla P) - c_1 P R + c_2 N_1 - c_3 N_1 P + c_4 N_2, \quad (3)$$

$$\frac{\partial R}{\partial t} = \nabla \cdot (\lambda_R M(\phi) \nabla R) - c_1 P R + c_2 N_1, \quad (4)$$

$$\phi = N_1 + N_2. \quad (5)$$

In Equations (1)—(5),  $0 < M(\phi) \leq 1$  is a non-dimensional phase-dependent term that scales the mobility. Additionally,  $F$  is the free energy of the system defined below in (6)—(7). To accommodate the two-component phase system, the model includes Ginsburg-Landau free

energy with a variation with a variation that transforms the classic double-well bulk chemical potential into an analogous well and trough (degenerate well)

$$F = \int_{\Omega} \frac{\varepsilon^2}{2} |\nabla(N_1 + N_2)|^2 + (N_1^2 + N_2^2)(1 - (N_1 + N_2))^2 dx, \quad (6)$$

where  $\varepsilon$  controls the interfacial thickness. To constrain the numerical stability, we add an extra stabilized term  $\alpha E$  into  $F$ , where  $E$  is given as

$$E(N_1, N_2) = \begin{cases} e^{-\gamma N_1}, & N_1 < 0, \\ e^{-\gamma N_2}, & N_2 < 0, \\ e^{-\gamma(1-N_1+N_2)}, & 1 - N_1 + N_2 < 0, \\ e^{-\gamma(1-N_2+N_1)}, & 1 - N_2 + N_1 < 0, \\ 0, & \text{otherwise,} \end{cases} \quad (7)$$

with  $\alpha$  and  $\gamma$  artificial numerical parameters. The heuristic free energy qualitatively matches the Standard Solution Model [18] without logarithmic singularities that constrain numerical stability. The logarithmic singularities are regularized by the function  $E(\cdot, \cdot)$ , which is defined outside the domain of definition of the volume fractions  $N_1, N_2$ .

## Results

The influence of reversible protein-RNA interactions on macroscopic phase field properties has been previously examined; here we explore and highlight the influence of protein-RNA interactions on *intra-droplet patterning* in space and time. For simplicity, we assume phase-independent mobility ( $M(\phi) = 1$ ): spatial movement would depend upon the diffusion rates ( $\lambda$ ) listed in Table 1. These diffusion constants are weighted relative to each other based on the molecular weights of an RNA (~1600 nucleotides) and protein (~78 kDa) that have been previously shown to undergo an RNA-dependent LLPS [25]. With this established set up, our analysis focuses on consequences of relative rates of protein-RNA binding-unbinding interactions.

Given previous work that modeled molecular interactions forming one phase separated protein-RNA complex, the initial aim of this model was to mimic a system driven by a single protein-RNA complex. The parameters in Table 1 were selected so the protein and RNA would bind quickly to form a stable  $N_1$  complex, a complex that would be slow to gain a second protein to form a stable  $N_2$  complex. This relationship creates an environment for  $N_1$  to accumulate quickly and thus initially resemble the single protein-RNA complex system. On a longer timescale, the slower formation of  $N_2$  complex leads to competition with  $N_1$  for resources.

As shown in Figure 2, at the onset of phase separation, the droplets are heavily populated with  $N_1$  at the center, while the  $N_2$  complex forms a ring at the droplet interface. As time progresses, the  $N_1$  complex continues to bind with free protein to form  $N_2$  and there is a wave-like diffusion of  $N_2$  inwards towards the droplet center. But, because the formation rate ( $c_1$ ) of the stable  $N_1$  complex is much faster than the rate of  $N_2$  formation,  $N_1$  still occupies the majority of each individual droplet as the system evolves towards a single-droplet system. This intra-droplet patterning of the system indicates that not only did  $N_1$  drive the phase separation but it is also the dominant phase-separated component as the system evolves. Next, we will explore the diversity of intra-droplet structure and dynamics as two key protein-RNA kinetic parameters are

varied: *the rates of  $N_1$  dissociation ( $c_2$ ) and  $N_2$  formation ( $c_3$ ), respectively.* Figure 2 is embedded as data point A in the state diagrams (at onset, intermediate time, and long-time) of Figure 3.

### *Altering binding kinetics alters droplet composition at phase separation onset*

To deviate from  $N_1$ -dominated droplets at the onset of phase separation, intuitively it is sufficient to impose a less-stable  $N_1$  complex and a quick-to-assemble and stable  $N_2$  complex by enhancing the rates of  $N_1$  disassociation ( $c_2$ ) and  $N_2$  formation ( $c_3$ ), respectively. Data point D in Figure 3 is a representative choice for this outcome. The influence of altering the rates of  $N_1$  disassociation ( $c_2$ ) and  $N_2$  formation ( $c_3$ ) at the onset of phase separation are shown in the state diagram in Figure 3A. For conditions where both  $c_2$  and  $c_3$  are small, the resulting product is a quickly forming, stable  $N_1$  complex and a slowly forming (yet stable)  $N_2$  complex, as shown in Figure 2. Thus, like in Figure 2,  $N_1$  occupies most of the droplets and exists at the droplet core. If the  $N_1$  complex is less stable (larger  $c_2$ ), but the  $N_2$  complex is too slow to form (low  $c_3$ ), the system is unable to phase separate. There simply is not enough of the needed protein-RNA complexes to drive and sustain phase separation.

If, however, both the rate of  $N_1$  disassociation ( $c_2$ ) and the rate of  $N_2$  formation ( $c_3$ ) are increased, the  $N_1$  complex forms for just long enough to quickly bind with nearby free protein, thus forming the stable  $N_2$  complex. This  $N_2$  complex will then be the dominant droplet component at the onset of phase separation. Thus, while varying  $c_2$  and  $c_3$  can result in a spectrum of droplet make-ups, the initial phase-separated behavior can be divided into three subcategories:  $N_1$ -dominated droplets with an  $N_1$  core,  $N_2$ -dominated droplets with an  $N_2$  core, or failure to phase separate.

### *Intra-droplet patterning evolves over multiple time scales*

In addition to altering the composition of the droplets at the onset of phase separation,  $c_2$  and  $c_3$  influence intermediate and long timescale intra-droplet patterning. The ( $c_2$ ,  $c_3$ ) state diagrams shown in Figures 3B and 3C show that the region of  $N_1$ -dominated droplets shrinks as  $t \rightarrow \infty$ . The boundary separating the  $N_1$ -dominated region from the  $N_2$ -dominated region shifts to the left, allowing for more  $N_2$ -dominated droplet systems long term. This shift means that, while the model started with two generalized states ( $N_1$ -core droplets vs.  $N_2$ -core droplets) at the onset of separation, the system can evolve to display 5 general behaviors of the droplets through time (Figure 4).

The intra-droplet pattern evolution behaviors are marked on the state diagrams as (A)-(E) and are mapped out explicitly in Figure 4. Systems with extreme initial behaviors, such as (A) and (D) in Figures 3 and 4, where one complex strongly dominates the droplets over the other at the onset of phase separation, are able to retain the same intra-droplet patterning as time progresses. It is the droplet systems near the dashed line in Figure 3A that experience changes in intra-droplet patterning. Droplet systems such as (B) in Figure 3 begin in an  $N_1$ -dominated droplet region, meaning that  $N_1$  exists at the core of the droplets. However, as time continues and the dashed line shifts, droplets evolve towards a single well-mixed droplet. In contrast, droplet systems on the other side of the dashed line in Figure 3A begin with an  $N_2$ -core and become increasingly  $N_2$  dominant as time progresses and the dashed line shifts.

Systems such as (E) begin with  $N_1$ -dominated droplets. However, as the dashed line in Figures 3B and 3C shifts, the system eventually has a single droplet with an  $N_2$  core and an  $N_1$  ring at the interface. Thus, it is possible for  $N_1$ -dominated droplet systems to evolve into an  $N_2$ -dominated droplet, so long as the system is comprised of a weak  $N_1$  complex and a quickly forming  $N_2$  complex.

### *Phase-Dependent Mobility Influences Long-Term Intra-Droplet Patterning, With Negligible Influence on Initial Phase Separation*

The droplets of biological phase-separated systems are more dense or concentrated than the surrounding solution [8, 25]. RNA, protein molecules, and complexes will experience a more viscous environment within phase-separated droplets, and, therefore, exhibit diminished diffusive mobility. In this section, we assume that the viscosity can be averaged according to the volume fraction of the mixture. Instead of the constant value of  $M(\phi) = 1$  used in the previous section, the mobility function,  $M(\phi)$ , is now scaled linearly with complex volume fraction in a phase-dependent manner, as shown in Equation (8), where  $m = M(1) - 1$ ,  $b = 1$ , and  $0 < M(\phi) \leq 1$ . With this new mobility function, diffusion within the droplet is reduced by a factor of  $10^3$  compared to the surrounding matrix.

$$M(\phi) = m \cdot \phi + b. \quad (8)$$

*The introduction of phase-dependent mobility does not drastically alter the composition of the droplets at the onset of phase separation.* Figure 5 shows the  $N_1$  location within the droplets for the five examples (A-E) highlighted in Figure 3, as well as the lack of phase separation (F), for both phase-independent and phase-dependent mobility. In all scenarios, the complex residing in the core at the time of phase separation with phase-independent mobility also dominates the core with phase-dependent mobility. Further, the time necessary for the system to phase separate does not shift with the phase-dependent mobility. Rather, as shown in Figure 6, it is the molecular interactions that control when the system phase separates. In particular, cases such as (D), where the  $N_1$  complex is weak and the  $N_2$  complex is slow to form, take the longest to phase separate. With the addition of phase-dependent mobility, in a well-mixed initial system,  $M(\phi)$  resembles phase-independent mobility, giving protein and RNA interactions control over system dynamics.

*Instead, the introduction of phase-dependent mobility influences the long-term patterning of the droplets.* Once the system phase separates, the phase-dependent mobility makes the inward movement of the shell complex much more difficult. One such example of this is in Figure 5A. With phase-independent mobility, as time progresses,  $N_1$  complexes at the interface of the droplet bind with free protein in the matrix, allowing the  $N_2$  population to grow and easily diffuse towards the droplet center. This diffusion increases the space  $N_2$  occupies in the single droplet system. However, with phase-dependent mobility, a larger single droplet traps proteins, RNAs, and complexes in the center. As the  $N_1$  complex slowly disassociates, it now has a pool of trapped, free protein available for binding and  $N_2$  complex formation. The result is the shell-ring-core (SRC) pattern that is observed in the phase-dependent mobility of Figure 5A at  $t = 1000$ . Shell-ring-core behavior also appears and is amplified in Figure 5D, where the  $N_1$  complex is unstable and the  $N_2$  complex is both quick to form and stable. This system initially depletes the free protein and RNA to form the  $N_2$  complex. With phase dependent mobility, however, a large, single droplet system traps free protein in the droplet core. While much of this free protein is used for  $N_2$  formation, its inability to escape also results in an increase in  $N_1$  concentration within the core, subsequently increasing the SRC behavior that faintly existed without phase-dependent mobility. Thus, in systems dominated by one complex, phase-dependent mobility allows for the weaker complex to grow and increase its long-term droplet presence.

Ultimately, the addition of phase-dependent mobility results in increased segregation of the protein-RNA complexes within all systems. As observed in Figure 7, the shell of the single



droplet in both systems A and D occupies less of the droplet radius with phase-dependent mobility than without at  $t = 1000$  due to the emergence of the shell-ring-core. Further, this increase in long-term complex segregation also persists in systems that are not heavily dominated by a single complex. While the complex dominating the shell in B, C, and E does not change, in Figure 7 the shells in these systems also occupy less of the droplet radius with phase-dependent mobility at  $t = 1000$  than without it. This decrease in droplet radius occupied by the shell indicates that, as the system evolves, the phase-dependent mobility forces the different complexes to mix and interact with each other less. Instead, phase-dependent mobility encourages further division of intra-droplet compartments.

## Discussion

We have shown that variations in intra-droplet patterning in time and space occur when different RNA-protein complexes draw from a common pool of components in a phase-separating system. In addition to setting up competition for common components, protein-RNA complex assembly and disassembly rates influence macroscopic phase field properties, including the time it takes to phase separate and the intra-droplet patterning and dynamics. We further show that variation of the kinetic rate constants leads to the emergence of shell-core intra-droplet patterning, establishing segregation of the different protein-RNA complexes within the droplets. Our model predicts that this patterning of the complexes within the droplet is a persistent construct that is maintained as the droplets undergo Ostwald ripening and evolve toward steady state behavior.

Even with the addition of phase-dependent mobility, the existence of intra-droplet patterning is persistent both at the onset of separation and in the long term. However, instead of the shell-core behavior created with phase-independent mobility, a more nuanced pattern within droplets emerges. In systems where the protein and RNA interactions dictate that one complex will drive and dominate during phase separation, the droplets evolve at different rates. Larger droplets create small microenvironments that trap free protein and RNA, creating a pool of free constituents within droplets to be used for new complex formation. The pool of trapped protein and RNA means that these systems evolve to a shell-ring-core behavior. Systems that are not dominated by one complex but instead depend on the exchange of free protein for complex creation do not have the long-term shell-ring-core behavior. Further, the shells in these droplets are smaller, a consequence of the phase-dependent mobility that further segregates the complexes within the droplet. These results predict that the rates of protein-RNA binding interactions establish the general intra-droplet patterning, while phase-dependent mobility dictates the details of patterns and their dynamics.

Intra-droplet patterning, e.g. shell-core behavior, has been observed previously [7, 26]. The creation and maintenance of this patterning could have significant biological implications on the function and material properties of these droplet condensates. Depending upon the interaction parameters, the complexes that exist on the surface can be varied in time and space. The availability of binding sites on the shell protein-RNA complex could determine how and when free protein and RNA diffuse into the droplets, as well as what species diffuse out of the droplet and into the surrounding fluid. This exchange of molecular components will influence the long-term composition of phase-separated droplets, their lifespan and ability to perform specific biochemistry inside or near the condensates. Likewise, the protein-RNA complex at the core of the droplets would have the free protein and RNA pools at its disposal, allowing for continued binding and rebinding, rather than relying on free constituents permeating from the ‘shell’.

Together, these behaviors could define the physical, observable properties of the droplets, as well as the role they play in the cell cytoplasm or nucleus.

The model presented in this work provides a theoretical scaffold for future model development. The appearance of the minor complex shell at the droplet interface implies that this complex may control or influence interactions that occur at the surface of the droplets. Given that it is possible for the minor and major complex to switch positions within the droplet by a reordering of the binding-unbinding rates, future experimental work is required to validate which droplet patterns are observed and persist over what timescales, and if patterns change, how they are tuned by post-translational modifications that would reorder binding-unbinding rates. Previous work has suggested that Ostwald ripening can be deterred if the system is kept from equilibrium [17, 19, 20]. A key difference between *in vitro* and *in vivo* conditions is the presence of protein and RNA synthesis and degradation, which may alter the way competition influences the dynamics of phase separation. With expansion of the model and future experiments, we aim to understand how the segregation and pattern formation of protein-RNA complexes can arise in physiological contexts. A key feature of biomolecular condensates is the formation of a surface which creates a boundary between the bulk and the condensed phase. This model presents a mechanism for this surface layer to have distinct properties and identity, which could, in turn, enable multiple functionalities within a single droplet. The degree to which droplets in cells exhibit, maintain or avoid the patterns predicted here presents an important area for future study.

## Figures

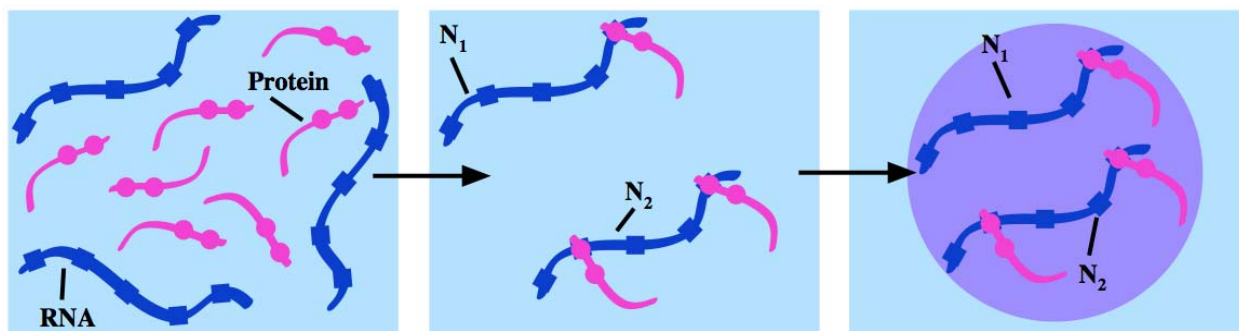


**Figure 1:** A single protein is capable of binding to a single RNA to form the  $N_1$  complex. The  $N_2$  complex is formed when an  $N_1$  complex acquires a second protein. The formation of protein-RNA complexes drives droplet formation and the  $N_1$  and  $N_2$  complexes are capable of mixing within a single droplet.

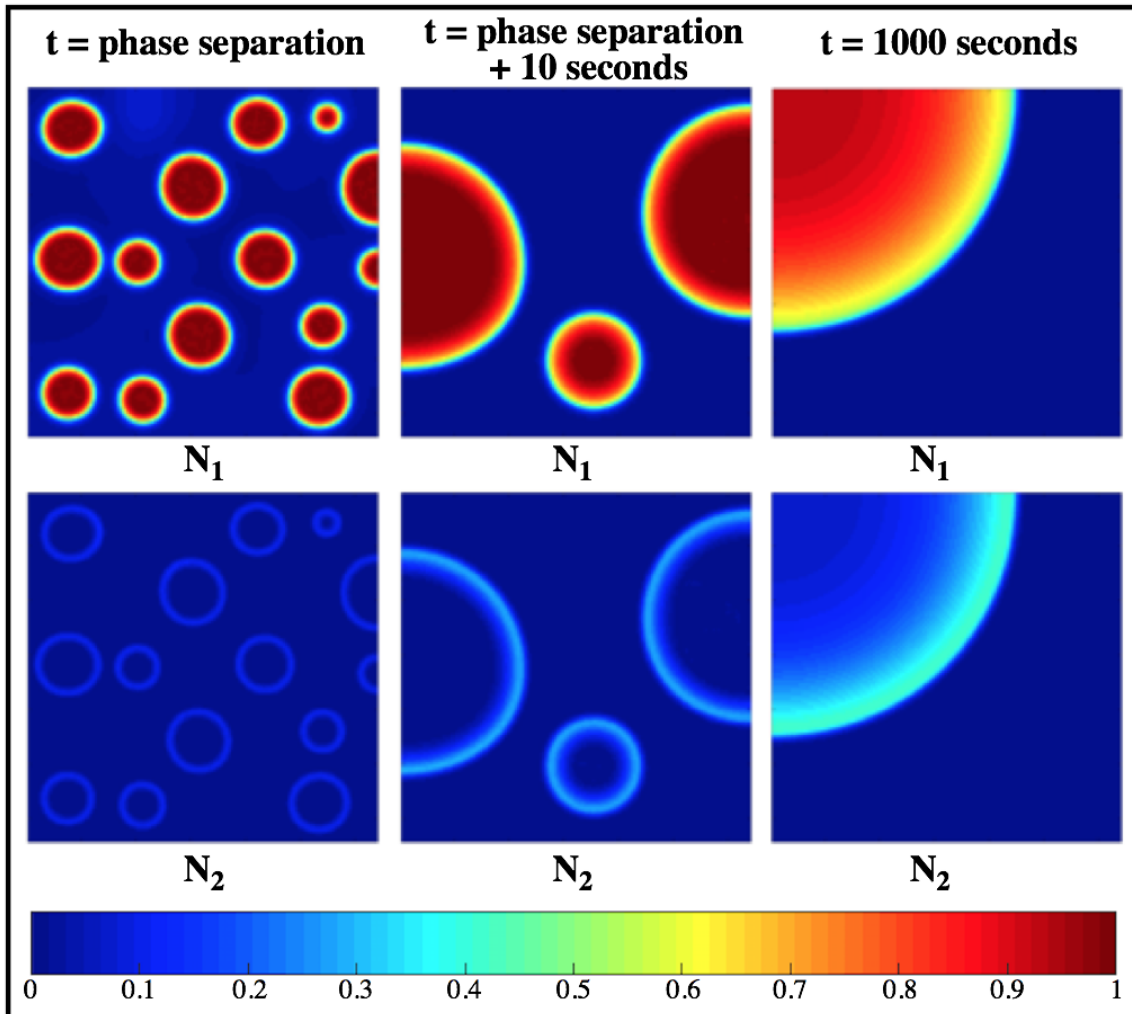


**Figure 2:** Initial droplet system and the location of  $N_1$  and  $N_2$  within the droplets at the time of phase separation, at the time of phase separation + 10 seconds, and at  $t = 1000$  seconds for the parameters outlined in Table 1.

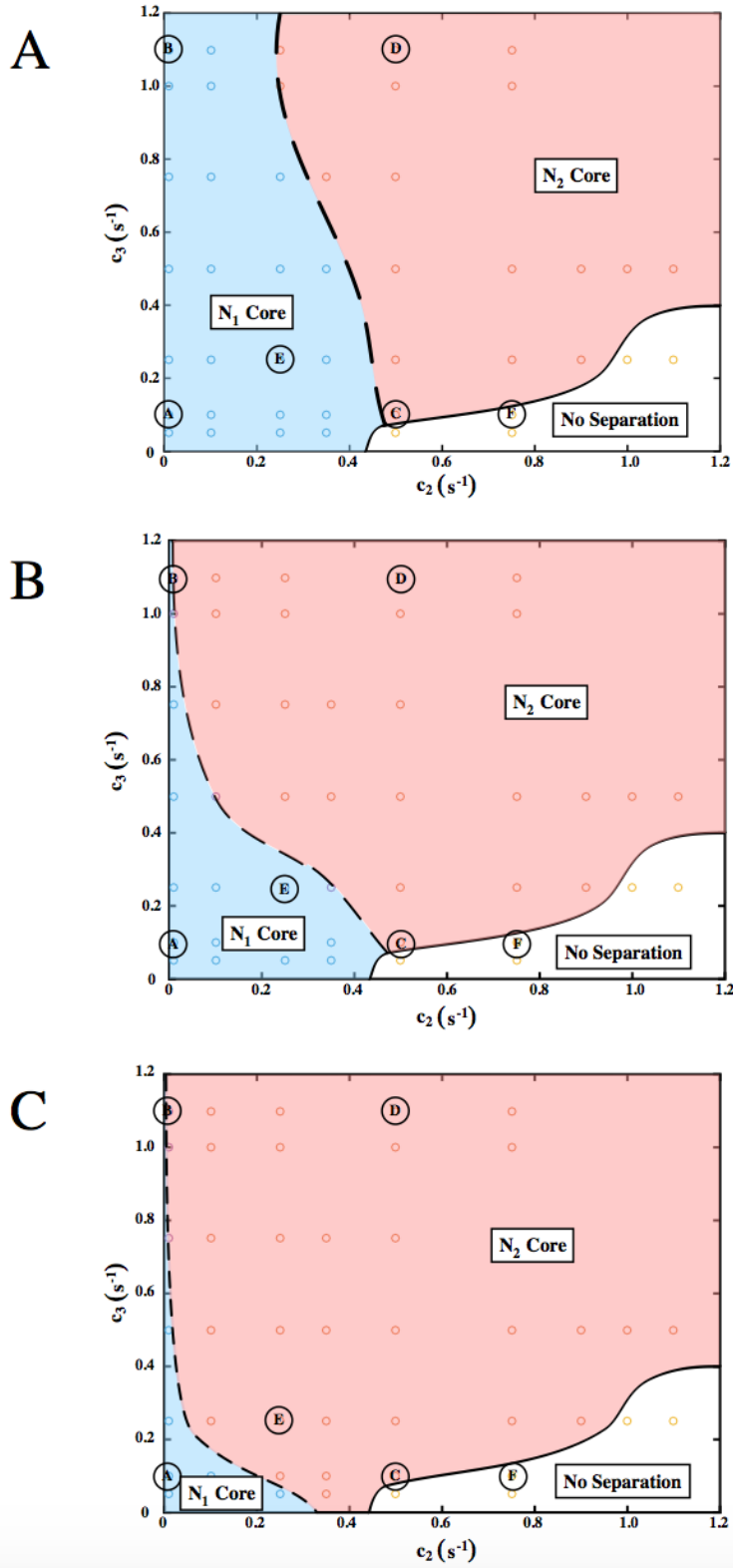


**Figure 3:** State diagrams of intra-droplet structure at three timescales versus the rate of  $N_1$  disassociation ( $c_2$ ) and  $N_2$  formation ( $c_3$ ). (A) At onset of phase separation. (B) At 10 seconds after the onset of phase separation. (C) At  $t = 1000$  seconds.

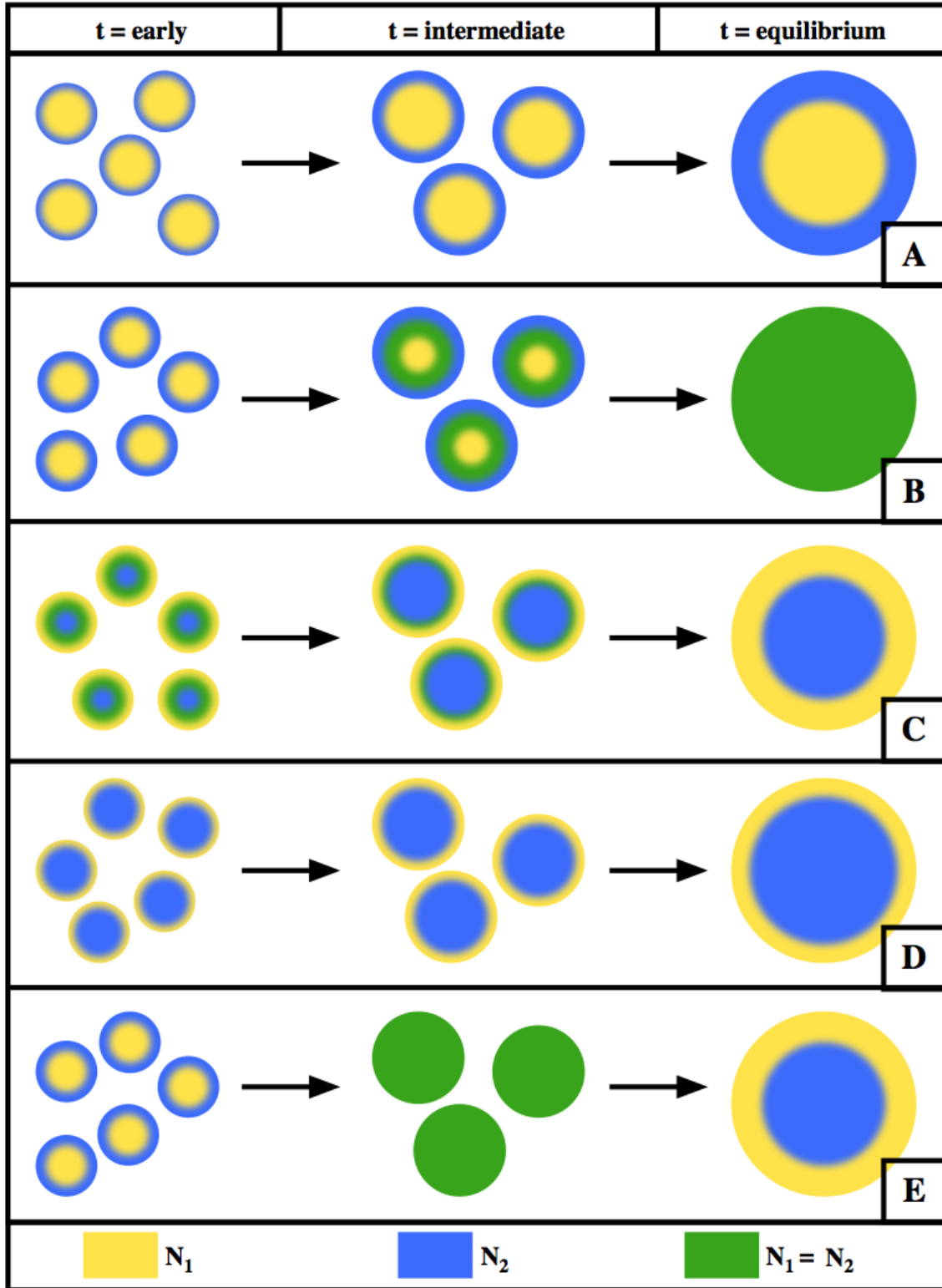


**Figure 4:** Five general cases for droplet evolution that correspond to the points (A-E) indicated in Figure 3. In each case, yellow indicates where  $N_1$  is located in the droplet while blue indicates where  $N_2$  is located. Green indicates that there is an even mixture of  $N_1$  and  $N_2$  (see color figure online).

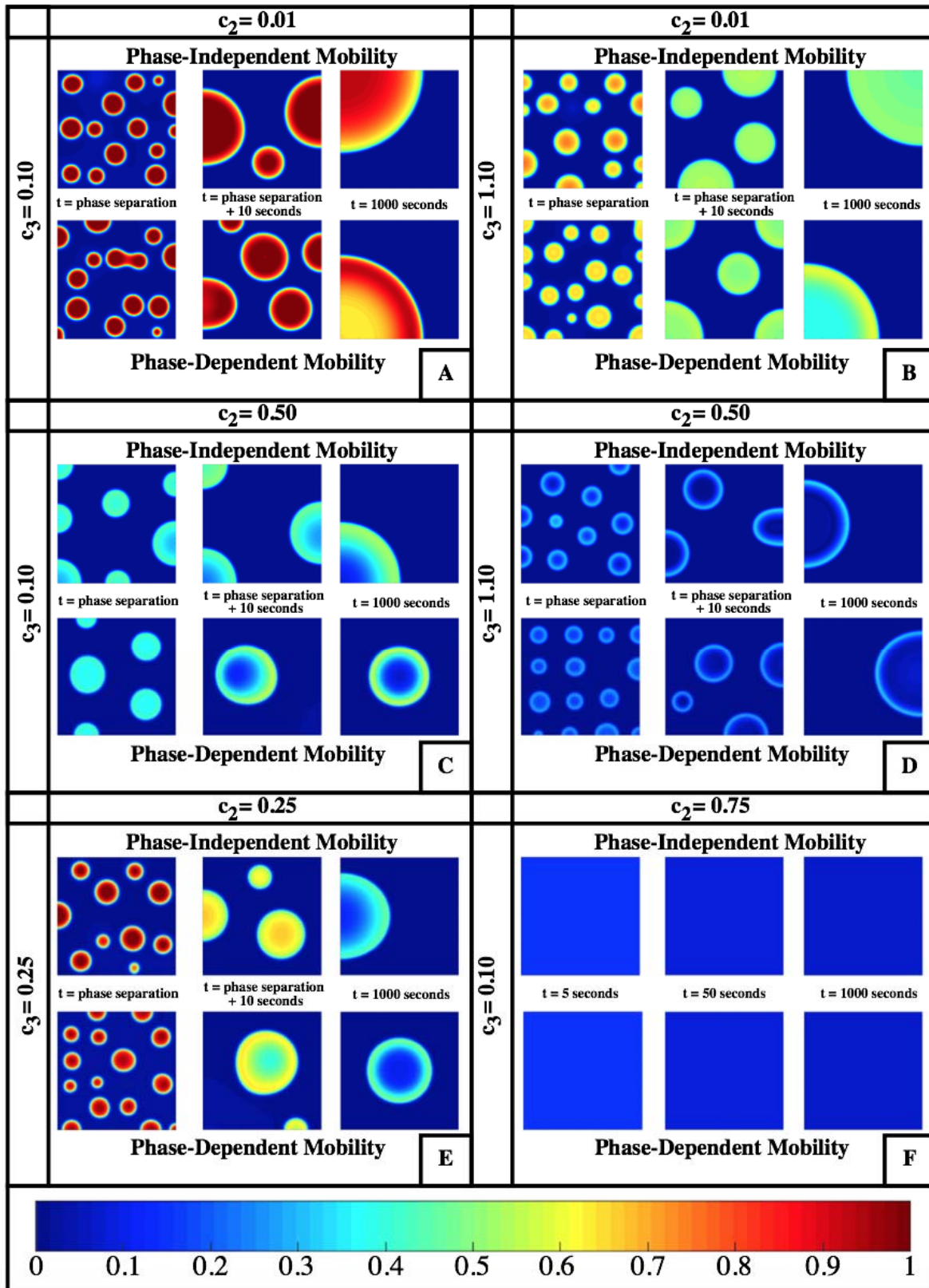


**Figure 5:** The location of  $N_1$  for both phase-independent mobility and phase-dependent mobility for examples corresponding to the points (A-F) indicated in Figure 3 (see color figure

online).

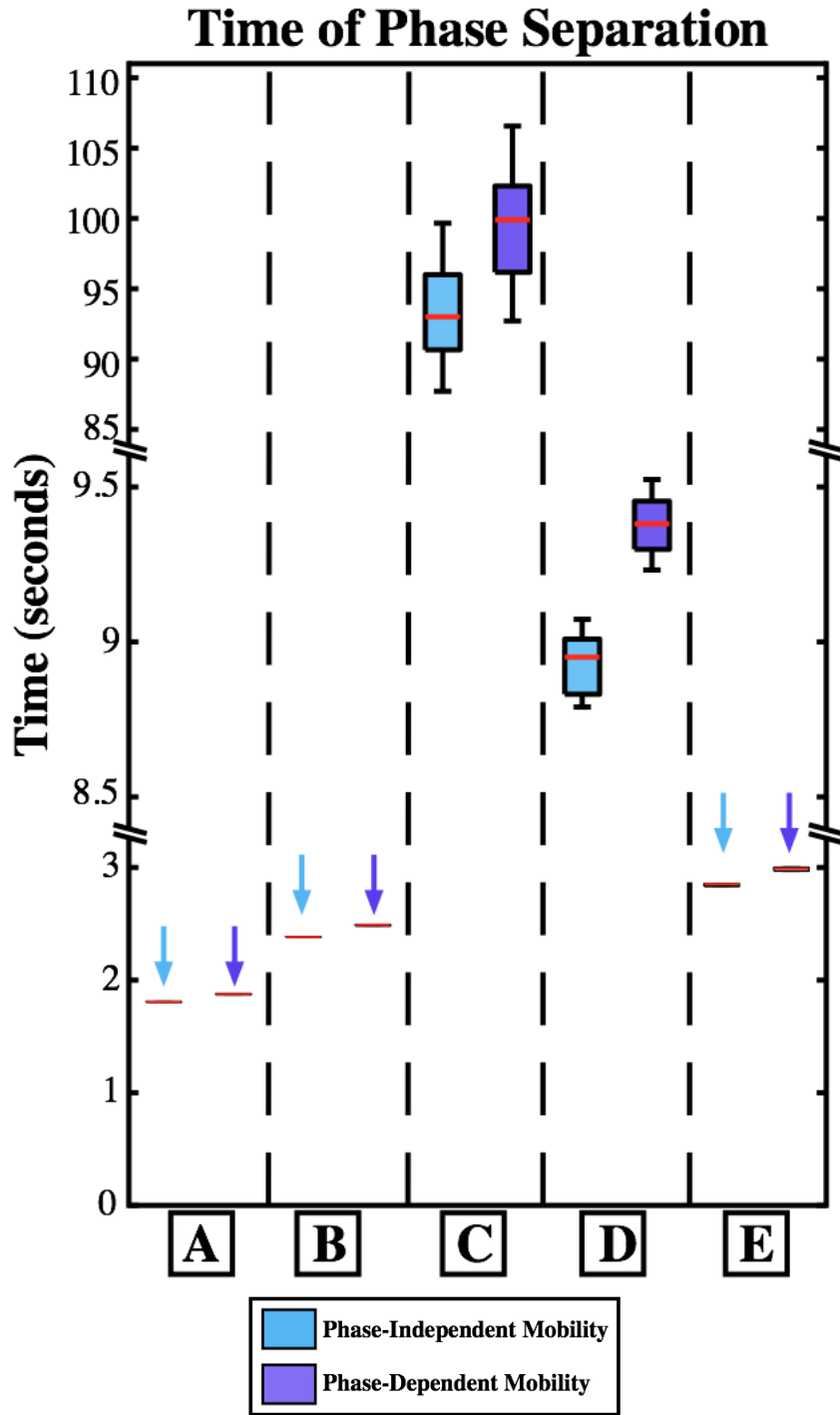


**Figure 6:** Time of phase separation for both phase-independent mobility and phase-dependent mobility corresponding to the points (A-E) indicated in Figure 3.

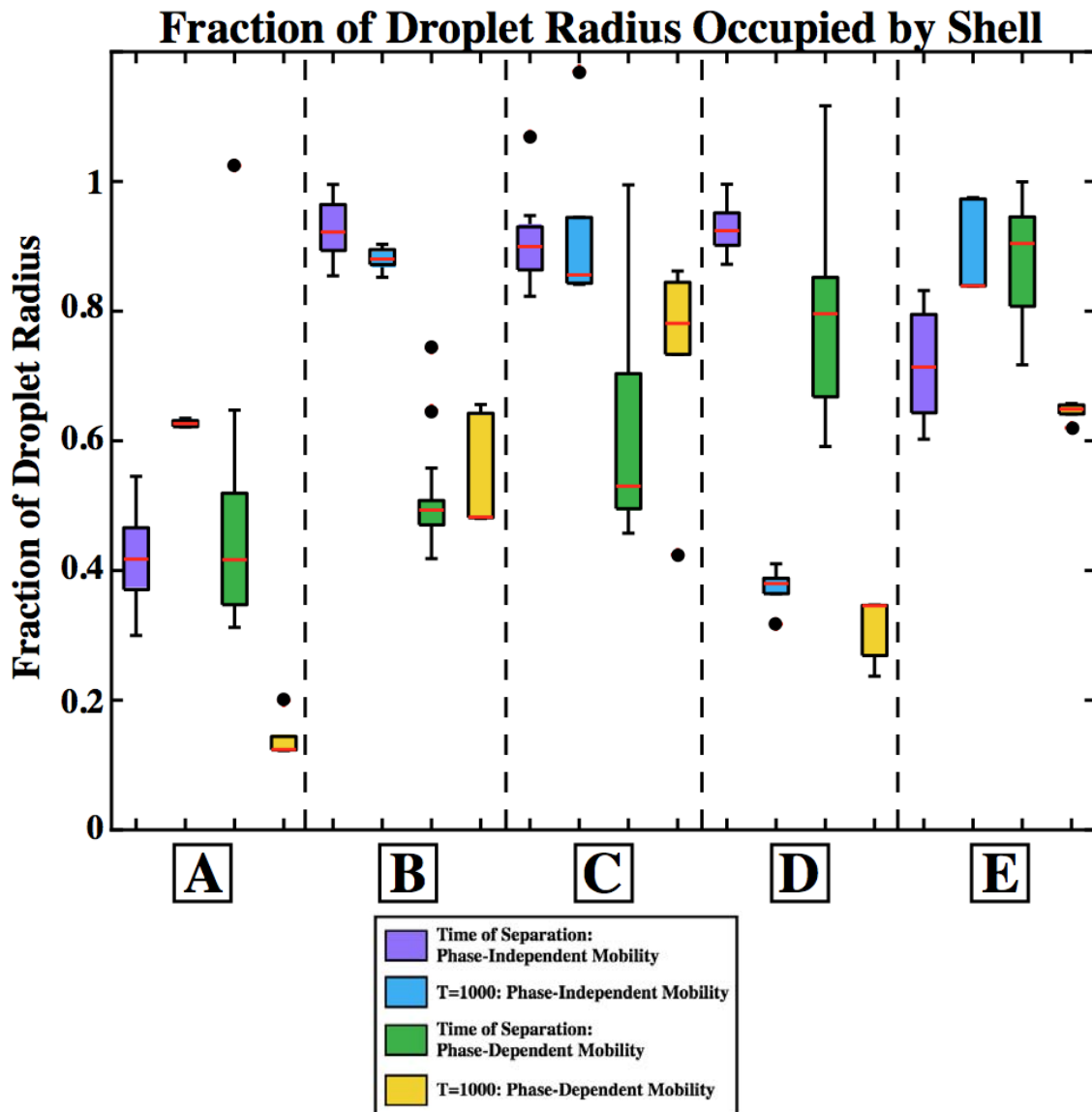


**Figure 7:** Fraction of the droplet radius occupied by the minority complex shell for both phase-independent mobility and phase-dependent mobility. A-E correspond to the points (A-E) indicated in Figure 3.



## Tables

Table 1: Parameter Definitions and Default Values for the Model			
Parameter	Definition	Value	Units
$\lambda_W$	Diffusion Rate of Free Protein	$3.75 \times 10^0$	$\frac{\mu m^2}{s}$
$\lambda_R$	Diffusion Rate of Free RNA	$5.8 \times 10^{-1}$	$\frac{\mu m^2}{s}$
$\lambda_{N_1}$	Diffusion Rate of $N_1$ Complex	$5 \times 10^{-1}$	$\frac{\mu m^2}{s}$
$\lambda_{N_2}$	Diffusion Rate of $N_2$ Complex	$4.4 \times 10^{-1}$	$\frac{\mu m^2}{s}$
$c_1$	Binding rate of Protein and RNA to form $N_1$	$1 \times 10^0$	$\frac{1}{s}$
$c_2$	Disassociation Rate of $N_1$	$1 \times 10^{-2}$	$\frac{1}{s}$
$c_3$	Binding rate of $N_1$ and Protein to form $N_2$	$1 \times 10^{-1}$	$\frac{1}{s}$
$c_4$	Disassociation rate of $N_2$ to release $N_1$ and Protein	$1 \times 10^{-2}$	$\frac{1}{s}$

## Bibliography

1. Weber SC, Brangwynne CP: **Getting RNA and protein in phase**. *Cell* 2012, **149**(6):1188-1191.
2. Langdon EM, Qiu Y, Niaki AG, McLaughlin GA, Weidmann C, Gerbich TM, Smith JA, Crutchley JM, Termini CM, Weeks KM: **mRNA structure determines specificity of a polyQ-driven phase separation**. *Science* 2018:eaar7432.
3. Nott TJ, Petsalaki E, Farber P, Jervis D, Fussner E, Plochowitz A, Craggs TD, Bazett-Jones DP, Pawson T, Forman-Kay JD: **Phase transition of a disordered nuage protein generates environmentally responsive membraneless organelles**. *Molecular cell* 2015, **57**(5):936-947.
4. Brangwynne CP, Tompa P, Pappu RV: **Polymer physics of intracellular phase transitions**. *Nature Physics* 2015, **11**(11):899-904.
5. Rai AK, Chen J-X, Selbach M, Pelkmans L: **Kinase-controlled phase transition of membraneless organelles in mitosis**. *Nature* 2018, **559**(7713):211.
6. Mitrea DM, Kriwacki RW: **Phase separation in biology; functional organization of a higher order**. *Cell Communication and Signaling* 2016, **14**(1):1.
7. Feric M, Vaidya N, Harmon TS, Mitrea DM, Zhu L, Richardson TM, Kriwacki RW, Pappu RV, Brangwynne CP: **Coexisting liquid phases underlie nucleolar subcompartments**. *Cell* 2016, **165**(7):1686-1697.

8. Elbaum-Garfinkle S, Kim Y, Szczepaniak K, Chen CC-H, Eckmann CR, Myong S, Brangwynne CP: **The disordered P granule protein LAF-1 drives phase separation into droplets with tunable viscosity and dynamics.** *Proceedings of the National Academy of Sciences* 2015, **112**(23):7189-7194.
9. Taylor N, Elbaum-Garfinkle S, Vaidya N, Zhang H, Stone HA, Brangwynne CP: **Biophysical characterization of organelle-based RNA/protein liquid phases using microfluidics.** *Soft matter* 2016, **12**(45):9142-9150.
10. Brangwynne CP: **Phase transitions and size scaling of membrane-less organelles.** *J Cell Biol* 2013, **203**(6):875-881.
11. Pak CW, Kosno M, Holehouse AS, Padrick SB, Mittal A, Ali R, Yunus AA, Liu DR, Pappu RV, Rosen MK: **Sequence determinants of intracellular phase separation by complex coacervation of a disordered protein.** *Molecular cell* 2016, **63**(1):72-85.
12. Lee C, Occhipinti P, Gladfelter AS: **PolyQ-dependent RNA-protein assemblies control symmetry breaking.** *J Cell Biol* 2015:jcb. 201407105.
13. Lee C, Zhang H, Baker AE, Occhipinti P, Borsuk ME, Gladfelter AS: **Protein aggregation behavior regulates cyclin transcript localization and cell-cycle control.** *Developmental cell* 2013, **25**(6):572-584.
14. Lin Y, Protter DS, Rosen MK, Parker R: **Formation and maturation of phase-separated liquid droplets by RNA-binding proteins.** *Molecular cell* 2015, **60**(2):208-219.
15. Zwicker D, Seyboldt R, Weber CA, Hyman AA, Jülicher F: **Growth and division of active droplets provides a model for protocells.** *Nature Physics* 2017, **13**(4):408.
16. Lee CF, Brangwynne CP, Gharakhani J, Hyman AA, Jülicher F: **Spatial organization of the cell cytoplasm by position-dependent phase separation.** *Physical review letters* 2013, **111**(8):088101.
17. Wurtz JD, Lee CF: **Chemical-Reaction-Controlled Phase Separated Drops: Formation, Size Selection, and Coarsening.** *Physical review letters* 2018, **120**(7):078102.
18. Berry J, Brangwynne CP, Haataja M: **Physical principles of intracellular organization via active and passive phase transitions.** *Reports on Progress in Physics* 2018, **81**(4):046601.
19. Glotzer SC, Di Marzio EA, Muthukumar M: **Reaction-controlled morphology of phase-separating mixtures.** *Physical review letters* 1995, **74**(11):2034.
20. Zwicker D, Hyman AA, Jülicher F: **Suppression of Ostwald ripening in active emulsions.** *Physical Review E* 2015, **92**(1):012317.
21. Hult C, Adalsteinsson D, Vasquez PA, Lawrimore J, Bennett M, York A, Cook D, Yeh E, Forest MG, Bloom K: **Enrichment of dynamic chromosomal crosslinks drive phase separation of the nucleolus.** *Nucleic Acids Research* 2017.
22. Cahn JW, Hilliard JE: **Free energy of a nonuniform system. I. Interfacial free energy.** *The Journal of chemical physics* 1958, **28**(2):258-267.
23. Qin R, Bhadeshia H: **Phase field method.** *Materials science and technology* 2010, **26**(7):803-811.
24. Fick A: **Ueber diffusion.** *Annalen der Physik* 1855, **170**(1):59-86.
25. Zhang H, Elbaum-Garfinkle S, Langdon EM, Taylor N, Occhipinti P, Bridges AA, Brangwynne CP, Gladfelter AS: **RNA controls PolyQ protein phase transitions.** *Molecular cell* 2015, **60**(2):220-230.

26. Jain S, Wheeler JR, Walters RW, Agrawal A, Barsic A, Parker R: **ATPase-modulated stress granules contain a diverse proteome and substructure**. *Cell* 2016, **164**(3):487-498.
27. Shen J, Yang X: **Numerical approximations of allen-cahn and cahn-hilliard equations**. *Discrete Contin Dyn Syst* 2010, **28**(4):1669-1691.
28. Gong Y, Zhao J, Wang Q: **Second Order Fully Discrete Energy Stable Methods on Staggered Grids for Hydrodynamic Phase Field Models of Binary Viscous Fluids**. *SIAM Journal on Scientific Computing* 2018, **40**(2):B528-B553.
29. Wise S: **Unconditionally stable finite difference, nonlinear multigrid simulation of the Cahn-Hilliard-Hele-Shaw system of equations**. *Journal of Scientific Computing* 2010, **44**(1):38-68.
30. Wise SM, Wang C, Lowengrub JS: **An energy-stable and convergent finite-difference scheme for the phase field crystal equation**. *SIAM Journal on Numerical Analysis* 2009, **47**(3):2269-2288.
31. See Supplementary Material at [] for supplementary videos (1-6). Supplementary videos (1-5) show the evolution of droplet systems (A-E) in Figure 3, respectively, up to  $t = 250$  seconds with phase-independent mobility. Supplementary video 6 shows the evolution of droplet system (A) in Figure 3 up to  $t = 250$  seconds with phase dependent mobility.

## Appendices

### Appendix 1: Numerical Schemes

In this section, we give the detailed numerical approximations for the LLPS model we proposed. Consider a rectangular domain  $\Omega = [0, L_x] \times [0, L_y]$ , where  $L_x$  and  $L_y$  is the length in x and y direction, respectively. The LLPS model is proposed as

$$\left\{ \begin{array}{l}
 \partial_t N_2 = \nabla \cdot \left( \lambda_{N_2} D(\phi) \nabla \frac{\delta F}{\delta N_2} \right) + c_3 N_1 - c_4 N_2, \quad \text{in } \Omega \times (0, T], \\
 \partial_t N_1 = \nabla \cdot \left( \lambda_{N_1} D(\phi) \nabla \frac{\delta F}{\delta N_1} \right) + c_1 P R - c_2 N_1 - c_3 N_1 P + c_4 N_2, \quad \text{in } \Omega \times (0, T], \\
 \partial_t P = \nabla \cdot \left( \lambda_P D(\phi) \nabla P \right) - c_1 P R + c_2 N_1 - c_3 N_1 P + c_4 N_2, \quad \text{in } \Omega \times (0, T], \\
 \partial_t R = \nabla \cdot \left( \lambda_R D(\phi) \nabla R \right) - c_1 P R + c_2 N_1, \quad \text{in } \Omega \times (0, T], \\
 \nabla \frac{\delta F}{\delta N_1} \cdot \mathbf{n} = 0, \nabla \frac{\delta F}{\delta N_2} \cdot \mathbf{n} = 0, \nabla N_1 \cdot \mathbf{n} = 0, \nabla N_2 \cdot \mathbf{n} = 0, \quad \text{on } \partial\Omega \times (0, T], \\
 \nabla P \cdot \mathbf{n} = 0, \nabla R \cdot \mathbf{n} = 0, \quad \text{on } \partial\Omega \times (0, T], \\
 N_1 = N_1^0, \quad N_2 = N_2^0, \quad P = P^0, \quad R = R^0 \quad \text{in } \Omega \times \{0\}.
 \end{array} \right. \quad (\text{A1.1})$$

In order to solve the LLPS model above, we use a second-order finite difference scheme for spatial discretization and second-order semi-implicit backward differential formula for time discretization. The stabilizing technique in [27] is also utilized during the time discretization.

We divide the domain into rectangular meshes with mesh size  $h_x = L_x/N_x$ ,  $h_y = L_y/N_y$  where  $N_x$  and  $N_y$  are the number of meshes in each direction. Then we define the sets of grid points in 1D as follows [28-30]

$$\begin{aligned} E_x &= \left\{x_{i+\frac{1}{2}} \mid i = 0, 1, \dots, N_x\right\}, & C_x &= \{x_i \mid i = 0, 1, \dots, N_x\}, \\ E_y &= \left\{y_{i+\frac{1}{2}} \mid i = 0, 1, \dots, N_y\right\}, & C_y &= \{y_i \mid i = 0, 1, \dots, N_y\}, \end{aligned} \quad (\text{A1.2})$$

where  $x_l = \left(l - \frac{1}{2}\right)h_x$  and  $y_l = \left(l - \frac{1}{2}\right)h_y$ . The sets  $E_x$  and  $E_y$  are the edge-centered points for the uniform partition, and  $C_x$  and  $C_y$  are the cell-centered points for the uniform partition.

We define the following discrete functional spaces:

$$C_{x \times y} = \{\phi: C_x \times C_y \rightarrow \mathbb{R}\}, \mathcal{E}_{x \times y}^{ew} = \{u: E_x \times C_y \rightarrow \mathbb{R}\}, \mathcal{E}_{x \times y}^{ns} = \{v: C_x \times E_y \rightarrow \mathbb{R}\}. \quad (\text{A1.3})$$

We define the center-to-east-west-edge average and difference operators  $A_x, D_x: C_{x \times y} \rightarrow \mathcal{E}_{x \times y}^{ew}$ :

$$A_x \phi_{i+\frac{1}{2}, j} = \frac{1}{2}(\phi_{i+1, j} + \phi_{i, j}), \quad D_x \phi_{i+\frac{1}{2}, j} = \frac{1}{h_x}(\phi_{i+1, j} - \phi_{i, j}). \quad (\text{A1.4})$$

We further define the center-to-north-south-edge average and difference operators  $A_y, D_y: C_{x \times y} \rightarrow \mathcal{E}_{x \times y}^{ns}$ :

$$A_y \phi_{i, j+\frac{1}{2}} = \frac{1}{2}(\phi_{i, j+1} + \phi_{i, j}), \quad D_y \phi_{i, j+\frac{1}{2}} = \frac{1}{h_y}(\phi_{i, j+1} - \phi_{i, j}). \quad (\text{A1.5})$$

Denote the full discrete Laplacian and biharmonic operators as:

$$\Delta_h = d_x(D_x \phi) + d_y(D_y \phi), \quad \Delta_h^2 = \Delta_h(\Delta_h). \quad (\text{A1.6})$$

With the notations above, the scheme for the LLPS model is given as follows.

**Scheme A1.1.** Give the initial condition  $N_1^0, N_2^0, P^0, R^0$ . After we obtain  $N_1^n, N_2^n, R^n, P^n$ ,  $n \geq 1$ , we can get  $(N_1^{n+1}, N_2^{n+1}, R^{n+1}, P^{n+1})$  via

$$\begin{aligned}
\delta_t^+ N_2^{n+1} &= \overline{d_x \cdot \left[ A_x \left( \lambda_{N_2} M(\phi) \right) D_x \left( \frac{\delta F}{\delta N_2} \right) \right]^{n+1}} + \overline{d_y \cdot \left[ A_y \left( \lambda_{N_2} M(\phi) \right) D_y \left( \frac{\delta F}{\delta N_2} \right) \right]^{n+1}} \\
&\quad - S_0 \Delta_h^2 \left( N_2^{n+1} - \overline{N_2}^{n+1} \right) + S_1 \Delta_h \left( N_2^{n+1} - \overline{N_2}^{n+1} \right) + \overline{f_{N_2}}^{n+1}, \\
\delta_t^+ N_1^{n+1} &= \overline{d_x \cdot \left[ A_x \left( \lambda_{N_1} M(\phi) \right) D_x \left( \frac{\delta F}{\delta N_1} \right) \right]^{n+1}} + \overline{d_y \cdot \left[ A_y \left( \lambda_{N_1} M(\phi) \right) D_y \left( \frac{\delta F}{\delta N_1} \right) \right]^{n+1}} \\
&\quad - S_0 \Delta_h^2 \left( N_1^{n+1} - \overline{N_1}^{n+1} \right) + S_1 \Delta_h \left( N_1^{n+1} - \overline{N_1}^{n+1} \right) + \overline{f_{N_1}}^{n+1}, \\
\delta_t^+ P^{n+1} &= \overline{d_x \cdot \left[ A_x \left( \lambda_P M(\phi) \right) D_x P \right]^{n+1}} + \overline{d_y \cdot \left[ A_y \left( \lambda_P M(\phi) \right) D_y P \right]^{n+1}} + S_P \Delta_h \left( P^{n+1} - \overline{P}^{n+1} \right) + \overline{f_P}^{n+1}, \\
\delta_t^+ R^{n+1} &= \overline{d_x \cdot \left[ A_x \left( \lambda_R M(\phi) \right) D_x R \right]^{n+1}} + \overline{d_y \cdot \left[ A_y \left( \lambda_R M(\phi) \right) D_y R \right]^{n+1}} + S_R \Delta_h \left( R^{n+1} - \overline{R}^{n+1} \right) + \overline{f_R}^{n+1},
\end{aligned}$$

where  $\delta_t(\cdot)^{n+1} = \frac{1}{2\delta t}(3(\cdot)^{n+1} - 4(\cdot)^n + (\cdot)^{n-1})$  is the second-order backward differential formula, and  $\overline{(\cdot)}^{n+1} = 2(\cdot)^n - (\cdot)^{n-1}$  is a second-order extrapolation, and  $S$ 's are stabilizing constants. Here,  $f$ 's are the reactive terms.

Note, the scheme above is decoupled, meaning  $N_1^{n+1}$ ,  $N_2^{n+1}$ ,  $P^{n+1}$ , and  $R^{n+1}$  could be solved independently. In each time step, the linear system for each variable could be solved efficiently by utilizing the fast cosine transform.

## Appendix 2: Steady State Behavior in a Well-Mixed System

Examining the steady state behavior of  $N_1$  and  $N_2$  in the ODE version of the system will allow us to understand how the long-term droplet make-up of  $N_1$  and  $N_2$  depends on the binding rates of the protein and RNA to form the RNP complexes. To find the steady state behavior of the ode system, the following condition must be satisfied:

$$\begin{cases} c_1 \cdot P \cdot R - c_2 \cdot N_1 = 0 \\ c_3 \cdot P \cdot N_1 - c_4 \cdot N_2 = 0 \end{cases} \quad (\text{A2.1})$$

Additionally, in this system, mass is conserved, meaning that

$$\begin{cases} P + N_1 + 0.5 \cdot N_2 = T_P \\ R + N_1 + N_2 = T_R \end{cases} \quad (\text{A2.2})$$

where the total volume fractions of protein and RNA are represented by  $T_P$  and  $T_R$ , respectively. Initially, in this system, protein-RNA complexes have yet to form and thus  $N_1(0) = N_2(0) = 0$ . Instead, half of the total initial volume fraction of the system is occupied by free protein and half is occupied by free RNA, meaning that  $T_P = T_R = 0.5$ . These conditions together result in two nullclines for  $N_1$  and one nullcline for  $N_2$ :

$$\begin{cases} N_{11} = \frac{1}{4c_1} \cdot \left( 2c_1 + 2c_2 - 3c_1N_2 - \sqrt{8c_1c_2 + 4c_2^2 - 12c_1c_2N_2 + c_1^2N_2^2} \right) \\ N_{12} = \frac{1}{4c_1} \cdot \left( 2c_1 + 2c_2 - 3c_1N_2 + \sqrt{8c_1c_2 + 4c_2^2 - 12c_1c_2N_2 + c_1^2N_2^2} \right) \\ N_2 = \frac{-0.5c_3N_1 + c_3N_1^2}{-c_4 - 0.5c_3N_1} \end{cases} \quad (\text{A2.3})$$

The nullclines in (A2.3) result in three steady states for the system: two imaginary solutions and one real solution. The real steady state solution for the system is shown below in (A2.4). While there is a single steady state that the volume fractions of  $N_1$  and  $N_2$  can achieve, note that the steady state values of both  $N_1$  and  $N_2$  rely on a relationship between all four binding rates:  $c_1$ ,  $c_2$ ,  $c_3$ ,  $c_4$ .

$$\begin{cases} N_1 = \frac{0.13(A + \sqrt{A^2 + 4B^3})^{1/3}}{c_3G} + \frac{1.33c_4H}{c_3G} - \frac{0.21B}{(A + \sqrt{A^2 + 4B^3})^{1/3}c_3G} \\ N_2 = -\frac{0.26K \left( K - 3.78c_3G(A + \sqrt{A^2 + 4B^3})^{1/3} \right)}{(A + \sqrt{A^2 + 4B^3})^{1/3}c_3G \left( K + 15.12c_4G(A + \sqrt{A^2 + 4B^3})^{1/3} \right)} \end{cases} \quad (\text{A2.4})$$

where  $A$ ,  $B$ ,  $G$ ,  $H$ , and  $K$  are defined as

$$\begin{aligned} A = & -72c_1^2c_2c_3^4c_4^2 + 360c_1c_2^2c_3^4c_4^2 - 16c_1^3c_3^3c_4^3 - 336c_1^2c_2c_3^3c_4^3 \\ & + 2112c_1c_2^2c_3^3c_4^3 + 128c_2^3c_3^3c_4^3 + 192c_1^3c_3^2c_4^4 \\ & - 3072c_1^2c_2c_3^2c_4^4 + 4224c_1c_2^2c_3^2c_4^4 - 768c_1^3c_3c_4^5 \\ & - 5376c_1^2c_2c_3c_4^5 + 1024c_1^3c_4^6, \end{aligned} \quad (\text{A2.5})$$

$$B = 48c_3c_4(c_2c_3 + 2c_1c_4)(0.125c_1c_3 + c_1c_4 + c_2c_4) - 64c_4^2(0.5c_1c_3 - c_2c_3 + c_1c_4)^2, \quad (\text{A2.6})$$

$$G = c_2c_3 + 2c_1c_4, \quad (\text{A2.7})$$

$$H = 0.5c_1c_3 - c_2c_3 + c_1c_4, \quad (\text{A2.8})$$

$$K = -1.59B + (A + \sqrt{A^2 + 4B^3})^{2/3} + 10.08c_4H(A + \sqrt{A^2 + 4B^3})^{1/3}. \quad (\text{A2.9})$$